Engineering Science & Technology
http://ojs.wiserpub.com/index.php/EST/

UNIVERSAL WISER PUBLISHER

Research Article

Analysis of Transient Buoyancy/Electroosmotic Driven Flow in a Vertical Microannulus with Velocity-Slip and Temperature-Jump

Michael O. Oni*, Basant K. Jha

Department of Mathematics, Ahmadu Bello University, Zaria, Nigeria
Email: michaeloni29@yahoo.com

Received: 21 December 2021; **Revised:** 13 January 2022; **Accepted:** 21 January 2022

Abstract: This article investigates the impact of electric body force on transient natural convection flow in a vertical microannulus with velocity slip and temperature jump. The governing momentum, energy, and Poisson-Boltzmann equations are presented for the current physical situation. The Laplace transform technique is employed to transform the governing partial differential equations into ordinary differential equations and then solved exactly in the Laplace domain using the method of undetermined coefficients. Line graphs and tables are simulated to properly explain the effects of various pertinent parameters on flow formation and temperature distribution. It is found that the time taken to attain a steady-state solution significantly depends on the slip-length and Electric Double Layer (EDL) length. In addition, the role of increasing the annular gap is to minimize the skin friction, electric field strength, and volumetric flow rate.

***Keywords*:** microannulus, velocity-slip, temperature-jump, electroosmotic flow

Nomenclature

C_0	concentration of ions in the bulk fluid
C_p, C_v	specific heats at constant pressure and constant volume, respectively (kJ/kgK)
E'_z	dimensional streaming potential (V/m)
E_z	dimensionless streaming potential (dimensionless)
F	Faraday's constant (dimensionless)
g	acceleration due to gravity (m/s^2)
Gr	Grashof number (dimensionless)
G_3	dimensionless parameter
I_0 and K_0	modified Bessel's function of first and second kind of order zero
Pr	Prandtl number
Q	dimensionless volume flow rate (dimensionless)
r	dimensional radial coordinate (m)
r_1	radius of the inner cylinder (m)
r_2	radius of the outer cylinder (m)

DOI: https://doi.org/10.37256/est.3120221293

R	dimensionless radial coordinate
R'	universal gas constant (kJ/kmol K)
s	Laplace parameter
t'	dimensional time (s)
t	dimensionless time (dimensionless)
T	dimensional temperature (K)
T_0	ambient fluid temperature (K)
T_1	temperature of the wall at $r = r_1$ (K)
T_2	temperature of the wall at $r = r_2$ (K)
$\hat{T}$	absolute temperature (K)
u	axial velocity (m/s)
U	dimensionless axial velocity (dimensionless)
$\overrightarrow{v}$	vectorial velocity profile (m/s)
Z'	valence number of ions in the solution (dimensionless)
z	dimensional axial coordinate (m)
Z	dimensionless axial coordinate

Greek letters

α'	dimensional velocity-slip length (m)
α	dimensionless velocity-slip length
δ'	dimensional temperature-jump length (m)
δ	dimensionless temperature-jump length
β	thermal expansion coefficient ($1/K$)
ε'	fluid permittivity (C/Vm)
ζ_1, ζ_2	dimensional zeta-potential (V)
$\hat{\zeta}_1, \hat{\zeta}_2$	dimensionless zeta-potential (dimensionless)
ζ_t	wall-ambient temperature difference ratio (dimensionless)
σ_t, σ_v	thermal and tangential momentum accommodation coefficients, respectively (dimensionless)
γ	ratio of specific heats (C_p/C_v) (dimensionless)
In	fluid-wall interaction parameter, β_t/β_v (dimensionless)
Γ	magnitude of electrokinetic effect (dimensionless)
ϕ	electrostatic potential (V)
Φ	externally imposed electrostatic potential (V)
κ	Debye-Hückel parameter (dimensionless)
k'	thermal conductivity (W/mK)
r^*	radii ratio (r_2/r_2) (dimensionless)
λ_D	Debye length (m)
ψ'	dimensional EDL potential (V)
ψ	dimensionless EDL potential (dimensionless)
μ	fluid dynamic viscosity (Ns/m^2)
ρ	fluid density (kg/m^3)
τ	skin-friction (dimensionless)
ν	kinematic viscosity (m^2/s)
ρ_e	charge density (C/m^3)
θ	dimensionless temperature

Subscripts

0	inlet properties of fluid at the entrance region
1	value on the surface $r = r_1$
2	value on the wall $r = r_2$
m	mean value

1. Introduction

With advances in science and technology, theoretical and experimental studies of microfluidics continue to gain scientists' attention. This is due to its applications in the manipulation of fluids to a small scale and the efficient design of heat and mass transfer systems. Some of the most common uses of microfluidics are the development of inkjet print heads, DNA chips, lab-on-a-chip technology, micro-propulsion, drug delivery to cancer patients, and micro-thermal technologies [1], [2]. Electroosmotic-based microfluidics has often been utilized for manipulating and controlling liquid flows in micro-devices [3]. Many theoretical and experimental contributions have been made in the study of electroosmotic flow to ascertain the impact of the electrokinetic phenomenon on pressure-driven flow formation and heat transfer in different microchannels. Some of the earliest works where experimental and theoretical analysis is carried out on the existence of electrokinetic phenomenon can be found respectively in Reuss [4] and Probstein [5]. After then, different physical situations on the electrokinetic phenomenon have been investigated both theoretically and experimentally. In microchannel, Mala et al. [6] gave experimental results on the flow of distilled water and aqueous solutions through silicon and glass microchannels between two parallel plates and found that the predicted volumetric flow rates agree with experimental data. Also, Mala et al. [7] examined the interfacial electrokinetic effects of the EDL at the solid-liquid interface on liquid flow and heat transfer through a microchannel between two parallel plates. Ren et al. [8] further investigated the electro-viscous effect caused by the EDL near a solid-liquid interface in microchannels while Zhang et al. [9] experimentally studied the streaming potentials across a porous membrane in various organic-aqueous solutions. In cylindrical geometries, Rice and Whitehead [10] theoretically investigated the electrokinetic flow in narrow cylindrical capillaries as an extension of Burgreen and Nakache [11] and concluded that the obtained analytical solutions are only valid for low electric potential. Later, Levine et al. [12] extended the work of Rice and Whitehead [10] by considering high zeta-potentials in microtubes. They obtained that flow formations for large EDL are significantly different from those of [10] for small EDL. After a few decades, Liechty et al. [13] numerically studied the fully developed convective heat transfer characteristics of electro-osmotically generated flow in microtubes at high wall potential. Their results clearly show that realistic values of the wall zeta potential produce thermal transport behavior which differs significantly from that predicted by an analysis employing the Debye-Hückel approximation [14]. Other related contributions where the combined pressure and electroosmotic flow are considered both in cylindrical and rectangular geometries are due to [15]-[20]. Usually, the EDL effects can be neglected for flows in microchannels since the EDL thickness is relatively small compared to the characteristic channel length. Whereas for flows in microchannels, the thickness of the EDL is comparable to the characteristic length of channels and its effect should be considered. It is known that the EDL effects originated from the interfacial electrokinetic effects by the variation of electric potential near a surface and could have a significant influence on the behavior of fluid flow [21].

The study of natural convection flow has been an interesting research field over the decades. This could be attributed to its cooling application of nuclear reactors, Micro-Electro-Mechanical-System (MEMS), and Nano-Electro-Mechanical Systems (NEMS). The natural convection flow is any flow-induced as a result of density difference caused by temperature difference. In microchannel and microtubes, several results have been obtained ranging from different physical situations to different boundary conditions [22]-[30].

Generally, flows in vertical geometries are often acted upon by the force of gravity [26], [28]. Also, unequal wall heating at the microannulus surfaces results in density difference thereby setting up natural convection current in the microchannel. This phenomenon has been widely neglected by researchers in the study of electroosmotic flow. Recently, an attempt was made by Khan et al. [31], where they investigated the mixed convection in a vertical channel in the presence of electrical double layers and found that the flow formation is slightly dependent on the Debye-Hückel

parameter. Although their work only considers the steady-state situations in the absence of velocity slip and temperature jump at the walls. Also, Oni and Jha [32] examined the impact of buoyant force as well as electroosmotic flow on laminar natural convection flow in a vertical microchannel. They established that the time required to attain the steady-state skin friction and mass flux is weakly dependent on EDL size while strongly dependent on slip parameters. Other related articles where the natural convection flow formation in microtubes and microannulus are carried out include Devi et al. [33], Goud et al. [34], Gai et al. [35], Rahmat et al. [36], Abdulrazzaq et al. [37]. Other recent contributions on the study of electroosmotic flow in different micro-geometries can be seen in [38]-[43]. In [33], it is found that the temperature gradient is an increasing function of the buoyancy force, while in [34], it is established that there is an increment in velocity and temperature based on an increment of heat source parameter.

Despite all these contributions, it is well known that flow formation and heat transfer in vertical microchannels are considerably different from those in microtubes, this is due to the difference in radius of curvature. This work aims to investigate the possibilities of exploiting a combination of both electrical potentials at the microannulus surfaces, electric body force, and buoyancy force to obtain optimized rates of microfluidic transport. The novelty of this current analysis is the development of mathematical functions to analyze the impact of buoyancy force on transient electroosmotic flow in a microannulus. This theoretical analysis has significant applications in electrohydrodynamics (especially in enhancement of batteries and separations at micro-level) when the experimental analysis is not readily achievable. The role of various governing parameters such as EDL length, Grashof number, slip-parameter, and pressure gradient is established with the aid of line graphs and tables.

2. Mathematical formulation

Consider an unsteady laminar fully developed electrokinetically driven natural convection flow of an incompressible, viscous fluid in a vertical micro-concentric-annulus. The z-axis is taken along the axis of the cylinders in the vertically upward direction and the r-axis is the radial direction. The radius of the inner and outer cylinders are r_1 and r_2 respectively, as shown in Figure 1. The outer surface of the inner cylinder is heated to a temperature (T_1), which is greater than that of the surrounding fluid having a temperature of T_0. The inner surface of the outer cylinder is maintained at a temperature (T_2) and asymmetric wall zeta-potentials ζ_1 and ζ_2. The charge distribution in the Electric-Double Layer (EDL) follows the Boltzmann distribution, therefore, the ion convection effects are negligible. Also, the wall potentials are considered low enough for Debye-Hückel linearization to be valid. The flow is assumed to be hydrodynamically and thermally fully developed, the viscous dissipation, compressibility effect of the fluid, and radiation effects are neglected. Further, the axial heat conduction in the fluid and on the walls is assumed to be negligible. Similarly, following Avci and Aydin [43], the usual continuum approach is applied by the continuum equations with the two main characteristics of the microscale phenomena; the velocity slip and the temperature jump.

2.1 *Governing equations*

The velocity slip at the surfaces of the micro-cylinder is defined as:

$$u_{s_1,s_2} = \pm\alpha' \left.\frac{\partial u}{\partial r}\right|_{r=r_1,r_2} \tag{1}$$

where u_{s_1} and u_{s_2} are the velocity slip on the surfaces of micro-annulus and α' is the dimensional slip-length. The temperature jump in a similar manner is defined as:

$$T_{s_1,s_2} - T_{w=1,2} = \pm\delta' \left.\frac{\partial T}{\partial r}\right|_{r=r_1,r_2} \tag{2}$$

where T_{s_1} and T_{s_2} are the temperatures of the fluid near the surfaces of micro-annulus, T_w is the temperature of the micro-annulus surfaces, and δ' is the dimensional thermal slip-length.

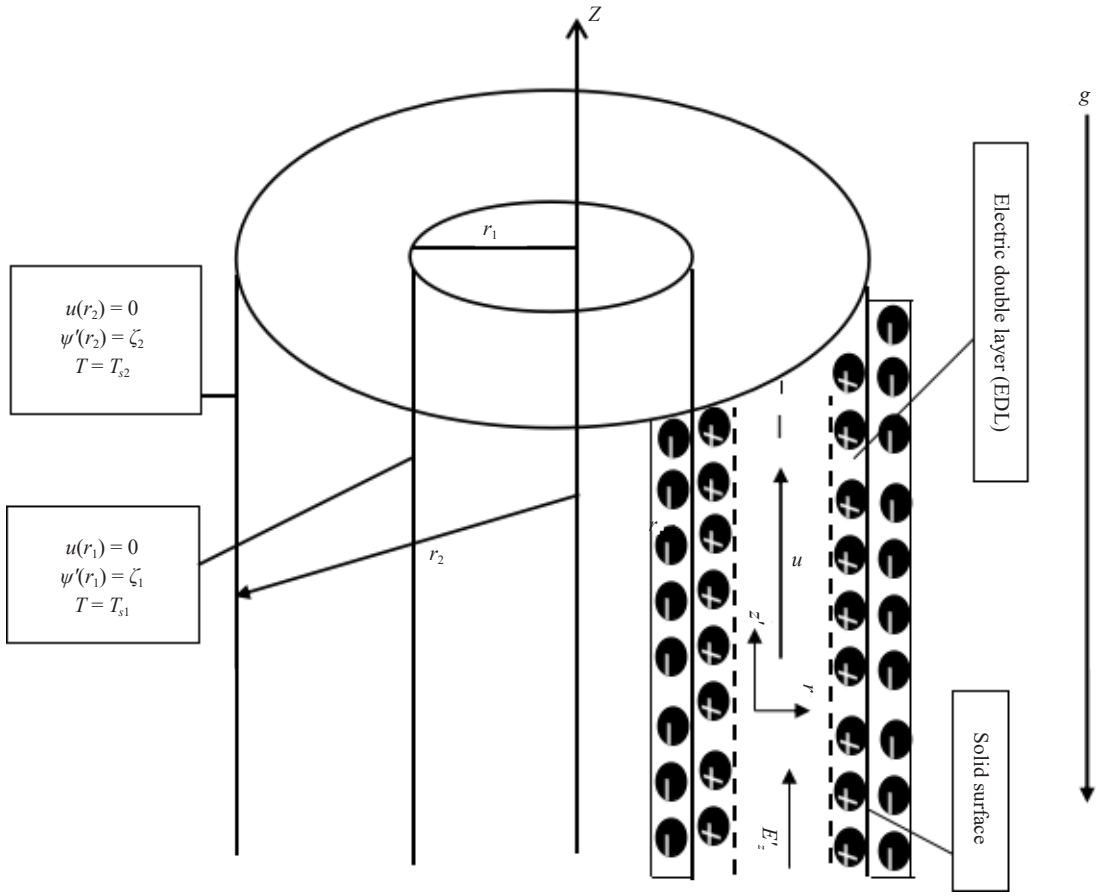

Figure 1. Schematic diagram of the problem

Following the stated assumptions, the governing electric potential, energy and momentum equations can be written respectively in dimensional form as follows:

$$\frac{1}{r}\frac{d}{dr}\left(r\frac{d\psi'}{dr}\right)=\frac{2FzC_0}{\varepsilon}\sinh\left(\frac{Z'F\psi'}{R'T}\right) \tag{3}$$

$$\frac{\partial T}{\partial t'}=\frac{k'}{\rho C_p}\frac{1}{r}\frac{\partial}{\partial r}\left(r\frac{\partial T}{\partial r}\right)+\frac{\mu}{\rho_0 C_p}\left(\frac{\partial u}{\partial r}\right)^2+\frac{E_z'^2}{\rho_0 C_p \sigma}\cosh^2\left(\frac{zF\psi'}{R'T}\right) \tag{4}$$

$$\frac{\partial u}{\partial t'}=\frac{\mu}{r}\frac{\partial}{\partial r}\left(r\frac{\partial u}{\partial r}\right)+\beta g\rho_0(T-T_0)+\rho_e E_z' \tag{5}$$

where ρ_0 is the mass density at temperature T_0 and T_0 is the reference fluid temperature which ensures a linear relation between the local mass density and local temperature. The last term of equation (5) represents the electrokinetic body force, which is obtained from the combination of applied electric gradient and EDL potential. While the last two terms in the energy equation (4) denote the viscous dissipation and Joule heating terms respectively. All other physical quantities employed in equations (3-5) are defined in nomenclature.

The reference temperature is chosen as the mean fluid temperature in any cross-section of the duct is defined as Avci and Aydin [43]:

$$T_0 = \frac{2}{r_2^2 - r_1^2}\int_{r_1}^{r_2} T(r) r\, dr \tag{6}$$

The boundary conditions are as follow:

$$t' \le 0, u = 0, T = T_0,$$

$$t' > 0, \begin{cases} \psi'(r) = \zeta_1, u = u_{s_1}, T = T_{s_1} & \text{at } r = r_1 \\ \psi'(r) = \zeta_2, u = u_{s_2}, T = T_{s_2} & \text{at } r = r_2 \end{cases} \tag{7}$$

Introducing the following dimensionless quantities and parameters:

$$R = \frac{r}{r_2}, r^* = \frac{r_1}{r_2}, D_h = 2(r_2 - r_1), \theta = \frac{T - T_0}{T_1 - T_2}, U = \frac{u}{u_m}, \alpha = \frac{\lambda}{D_h}, P_r = \frac{\mu C_p}{k'}, w = \frac{T_1 - T_0}{T_1 - T_2},$$

$$Gr = \frac{g\beta(T_1 - T_2)D_h^3}{v^2}, \xi_1^* = \frac{Z'F\xi_1}{R'\hat{T}}, \xi_2^* = \frac{Z'F\xi_2}{R'\hat{T}}, \Gamma = \frac{\varepsilon R'\hat{T}\xi}{Z'F\rho_0 v^2}, E_z = \frac{E_z' H}{\xi}, t = \frac{vt'}{D_h^2}, S = \frac{1}{\sigma_0(T_1 - T_2)}$$

$$Br = \frac{\mu {u_m}^2}{\kappa'(T_w - T_0)}, A = [2(1 - r^*)]^2, \kappa = \frac{D_h}{\lambda_D}, \lambda_D = \left[\frac{\varepsilon_0 \varepsilon' k_b \hat{T}}{2e^2 z'^2 n_0}\right]^{1/2} \tag{8}$$

Applying Debye-Hückel linearization on equations (3 and 5), and using equation (8), equations (1-7) can be written respectively in dimensionless form as:

$$\frac{1}{R}\frac{d}{dR}\left(R\frac{d\psi}{dR}\right) - \frac{\kappa^2}{A}\psi = 0 \tag{9}$$

$$\frac{Pr}{A}\frac{\partial\theta}{\partial t} = \frac{1}{R}\frac{\partial}{\partial R}\left(R\frac{d\theta}{\partial R}\right) + \frac{Br}{A}\left[\left(\frac{\partial U}{\partial R}\right)^2 + S{E_z}^2\right] \tag{10}$$

$$\frac{1}{A}\frac{\partial U}{\partial t} = \frac{1}{R}\frac{\partial}{\partial R}\left(R\frac{dU}{dR}\right) + \frac{1}{A}\left[Gr\theta - \kappa^2\Gamma E_z\psi\right] \tag{11}$$

The boundary conditions which describe the velocity slip and temperature jump conditions at the fluid wall interface in the dimensionless form are:

$$\text{At } t \le 0, U = 0, \theta = 0,$$

$$t > 0 \begin{cases} \psi(R) = \zeta_1^*, U = \alpha\dfrac{dU}{dR}, \theta = w + \delta\dfrac{d\theta}{dR}, & at \;\; R = r^* \\ \psi(R) = \zeta_2^*, U = -\alpha\dfrac{dU}{dR}, \theta = w - 1 - \delta\dfrac{d\theta}{dR}, & at \;\; R = 1 \end{cases} \tag{12}$$

The nonlinear partial differential equations (9-11) with boundary conditions (12) give the mathematical model

governing the time-dependent mixed convection flow formation in a vertical microannulus with an electrokinetic effect. It is well known that electroosmotic flow behaves as a plug flow (low velocity) so that the viscous dissipation term in equation (10) is negligible. In addition, for low wall potentials, the Joule heating term becomes a constant so that neglecting the Joule heating term does not distort the physics of flow formation.

Based on the aforementioned assumptions, and applying the Laplace transform technique to transform the governing partial differential equations into ordinary differential equations as follows:

$$\overline{U}(Y,s)=\int_0^\infty U(Y,t)e^{-st}dt \text{ and } \overline{\theta}(Y,s)=\int_0^\infty \theta(Y,t)e^{-st}dt \tag{13}$$

where $s > 0$ is the Laplace transform parameter.

By applying equation (13), the governing electric potential, energy and momentum equations governing flow formation and temperature distribution are given as:

$$\frac{1}{R}\frac{d}{dR}\left(R\frac{d\psi}{dR}\right)-\frac{\kappa^2}{A}\psi=0 \tag{14}$$

$$\frac{1}{R}\frac{d}{dR}\left(R\frac{d\overline{\theta}}{dR}\right)-\frac{sPr}{A}\overline{\theta}=0 \tag{15}$$

$$\frac{1}{R}\frac{d}{dR}\left(R\frac{d\overline{U}}{dR}\right)-\frac{1}{A}[Gr\overline{\theta}-\kappa^2\Gamma E_z\psi]-\frac{s}{A}\overline{U} \tag{16}$$

Subject to

$$\begin{gathered}\psi(R)=\zeta_1^*,\ \overline{U}=\alpha\frac{d\overline{U}}{dR},\ \overline{\theta}=\frac{w}{s}+\delta\frac{d\overline{\theta}}{dR},\ \ at\ R=r^*\\ \psi(R)=\zeta_2^*,\ \overline{U}=-\alpha\frac{d\overline{U}}{dR},\ \overline{\theta}=\frac{(w-1)}{s}-\delta\frac{d\overline{\theta}}{dR},\ \ at\ R=1\end{gathered} \tag{17}$$

2.2 *Analytical solution*

Solving equations (14-16) with boundary conditions (17) using the method of undetermined coefficients, we have the closed-form solutions for the electric potential, temperature distributions and velocity respectively in the Laplace domain in term of modified Bessel's function of first and second kinds of order zero as:

$$\psi(R)=C_1I_0\left(\frac{R\kappa}{\sqrt{A}}\right)+C_2K_0\left(\frac{R\kappa}{\sqrt{A}}\right) \tag{18}$$

$$\overline{\theta}(R,s)=C_3I_0\left(R\sqrt{\frac{sPr}{A}}\right)+C_4K_0\left(R\sqrt{\frac{sPr}{A}}\right) \tag{19}$$

$$\overline{U}(R,s)=C_5I_0\left(R\sqrt{\frac{s}{A}}\right)+C_6K_0\left(R\sqrt{\frac{s}{A}}\right)+\frac{E_z\Gamma\kappa^2}{s(\kappa^2-s)}\left[C_1I_0\left(\frac{R\kappa}{\sqrt{A}}\right)+C_2K_0\left(\frac{R\kappa}{\sqrt{A}}\right)\right]$$

$$-\frac{Gr}{s(Pr-1)}\left[C_3 I_0\left(R\sqrt{\frac{sPr}{A}}\right)+C_4 K_0\left(R\sqrt{\frac{sPr}{A}}\right)\right] \tag{20}$$

where I_0 and K_0 are the modified Bessel's function of first and second kind of order zero, and C_1 – C_6 are constants defined as:

$$C_1=\frac{\xi_2^* K_0(r^*\delta_1)-\xi_1^* K_0(\delta_1)}{I_0(\delta_1)K_0(r^*\delta_1)-I_0(r^*\delta_1)K_0(\delta_1)},$$

$$C_2=\frac{\xi_1^* I_0(r^*\delta_1)-\xi_2^* I_0(\delta_1)}{I_0(\delta_1)K_0(r^*\delta_1)-I_0(r^*\delta_1)K_0(\delta_1)},$$

$$C_3=\frac{X_6X_2-X_3X_5}{X_4X_2-X_1X_5},$$

$$C_4=\frac{X_3X_4-X_1X_6}{X_4X_2-X_1X_5},$$

$$C_5=\frac{X_{12}X_{15}+E_z(X_{13}X_{15}-X_{17}X_{11})-X_{16}X_{11}}{X_{10}X_{15}-X_{14}X_{11}},$$

$$C_6=\frac{X_{10}X_{16}+E_z(X_{10}X_{17}-X_{13}X_{14})-X_{14}X_{12}}{X_{10}X_{15}-X_{14}X_{11}} \tag{21}$$

where X_1, X_2, X_3, ... are constants defined in the Appendix.

The skin-frictions at the surfaces of the microannulus $R = r^*$ and $R = 1$ are respectively obtained in Laplace domain as:

$$\bar{\tau}_{r^*}=\left.\frac{d\bar{U}(R,s)}{dR}\right|_{R=r^*}=\sqrt{\frac{s}{A}}\left[C_5 I_1\left(r^*\sqrt{\frac{s}{A}}\right)-C_6 K_1\left(r^*\sqrt{\frac{s}{A}}\right)\right]$$

$$+\frac{E_z\Gamma\kappa^3\left[C_1 I_1\left(\frac{r^*\kappa}{\sqrt{A}}\right)-C_2 I_1\left(\frac{r^*\kappa}{\sqrt{A}}\right)\right]}{\sqrt{A}s(\kappa^2-s)}-\frac{Gr\sqrt{sPr}\left[C_3 I_1\left(r^*\sqrt{\frac{sPr}{A}}\right)-C_4 K_1\left(r^*\sqrt{\frac{sPr}{A}}\right)\right]}{\sqrt{A}s(Pr-1)} \tag{22}$$

$$\bar{\tau}_1=\left.\frac{d\bar{U}(R,s)}{dR}\right|_{R=1}=\sqrt{\frac{s}{A}}\left[C_5 I_1\left(\sqrt{\frac{s}{A}}\right)-C_6 K_1\left(\sqrt{\frac{s}{A}}\right)\right]$$

$$+\frac{E_z\Gamma\kappa^3\left[C_1 I_1\left(\frac{\kappa}{\sqrt{A}}\right)-C_2 I_1\left(\frac{\kappa}{\sqrt{A}}\right)\right]}{\sqrt{A}s(\kappa^2-s)}-\frac{Gr\sqrt{sPr}\left[C_3 I_1\left(\sqrt{\frac{sPr}{A}}\right)-C_4 K_1\left(\sqrt{\frac{sPr}{A}}\right)\right]}{\sqrt{A}s(Pr-1)} \tag{23}$$

Also, the dimensionless volumetric flow rate in the Laplace domain is given by:

$$\overline{Q} = \int_0^1 R\overline{U}(R,s)dR = \sqrt{\frac{A}{s}}\left[C_5\left(I_1\left(\sqrt{\frac{s}{A}}\right) - r^* I_1\left(r^*\sqrt{\frac{s}{A}}\right)\right) - C_6\left(K_1\left(\sqrt{\frac{s}{A}}\right) - r^* K_1\left(r^*\sqrt{\frac{s}{A}}\right)\right)\right]$$

$$+\frac{E_z \Gamma \kappa\sqrt{A}\left[C_1\left(I_1\left(\frac{\kappa}{\sqrt{A}}\right) - r^* I_1\left(\frac{r^*\kappa}{\sqrt{A}}\right)\right) - C_2\left(K_1\left(\frac{\kappa}{\sqrt{A}}\right) - r^* K_1\left(\frac{r^*\kappa}{\sqrt{A}}\right)\right)\right]}{s(\kappa^2 - s)}$$

$$-\frac{Gr\left[C_3\left(I_1\left(\sqrt{\frac{sPr}{A}}\right) - r^* I_1\left(r^*\sqrt{\frac{sPr}{A}}\right)\right) - C_4\left(K_1\left(\sqrt{\frac{sPr}{A}}\right) - r^* K_1\left(r^*\sqrt{\frac{sPr}{A}}\right)\right)\right]}{\sqrt{sPr}\,s(Pr-1)} \tag{24}$$

2.3 *Riemann-Sum Approximation (RSA)*

The analytical solutions obtained in equations (19-24) are in the Laplace domain. Meanwhile, the mathematical models presented in equations (10-12) are in the time domain. Therefore, the solutions obtained above need to be transformed to the time domain for a better understanding of flow formation. Due to the difficulty in transforming the closed-form expressions obtained in the Laplace domain to the time-domain, a numerical Laplace inversion technique employed in [44]-[47], which is based on the Riemann-Sum Approximation (RSA), is employed. This numerical Laplace inversion technique has proven to be accurate and reliable in solving time-dependent problems [45]. The temperature distribution, velocity profile, skin-friction, and mass-flux which are in the Laplace domain are inverted to the time domain respectively as follows:

$$\theta(R,t) = \frac{e^{\varepsilon t}}{t}\left[\frac{1}{2}\overline{\theta}(R,\varepsilon) + Re\sum_{n=1}^{M}\overline{\theta}\left(R,\varepsilon + \frac{in\pi}{t}\right)(-1)^n\right], r^* \le R \le 1 \tag{25}$$

$$U(R,t) = \frac{e^{\varepsilon t}}{t}\left[\frac{1}{2}\overline{U}(R,\varepsilon) + Re\sum_{n=1}^{M}\overline{U}\left(R,\varepsilon + \frac{in\pi}{t}\right)(-1)^n\right], r^* \le R \le 1 \tag{26}$$

$$\tau(r^*,t) = \frac{e^{\varepsilon t}}{t}\left[\frac{1}{2}\overline{\tau}(0,\varepsilon) + Re\sum_{n=1}^{M}\overline{\tau}\left(0,\varepsilon + \frac{in\pi}{t}\right)(-1)^n\right], R = r^* \tag{27}$$

$$\tau(1,t) = \frac{e^{\varepsilon t}}{t}\left[\frac{1}{2}\overline{\tau}(1,\varepsilon) + Re\sum_{n=1}^{M}\overline{\tau}\left(1,\varepsilon + \frac{in\pi}{t}\right)(-1)^n\right], R = 1 \tag{28}$$

$$Q(t) = \frac{e^{\varepsilon t}}{t}\left[\frac{1}{2}\overline{Q}(\varepsilon) + Re\sum_{n=1}^{M}\overline{Q}\left(\varepsilon + \frac{in\pi}{t}\right)(-1)^n\right], \tag{29}$$

where Re denotes the real part, $i = \sqrt{-1}$ the imaginary number. M is the number of terms used in the Riemann-sum approximation and ε is the real part of the Bromwich contour that is used in inverting Laplace transforms. The convergence of the solution depends on the value of ε and the truncation error dictated by M. According to Tzo [47] and based on inspection, the value of εt that best satisfied the result is 4.7. Equations (25-29) above give the mathematical models governing transient temperature, velocity, skin friction at the surfaces of the microannulus, and volumetric flow

rate, respectively.

2.4 *Steady-State Solution (SSS)*

For analysis of the role of electric body force on flow formation, it is noteworthy to compute the steady-state value of velocity profile and temperature distributions in the vertical microannulus as it helps to validate the accuracy of the Riemann-sum approximation approach employed in equations (25-29). The SSS is obtained by substituting $\frac{\partial()}{\partial t} = 0$ in equations (10) and (11) and solving the ordinary differential equation under relevant boundary conditions. The temperature distribution and velocity profile at steady-state solutions are respectively obtained as:

$$\theta(R) = C_7 \ln R + C_8 \tag{30}$$

$$U(R) = C_9 \ln R + C_{10} + \frac{E_z \Gamma}{s(\kappa^2 - s)}\left[C_1 I_0\left(\frac{R\kappa}{\sqrt{A}}\right) + C_2 K_0\left(\frac{R\kappa}{\sqrt{A}}\right)\right] - \frac{Gr}{A}\left[\frac{C_7 R^2}{4}(\ln R - 1) + C_8 \frac{R^2}{4}\right] \tag{31}$$

The skin-frictions at the surfaces of the micro-annulus at the steady-state are given as:

$$\tau_{r^*} = \left.\frac{dU(R)}{dR}\right|_{R=r^*} = \frac{C_9}{r^*} + \frac{E_z \Gamma \kappa}{\sqrt{A}}\left[C_1 I_1\left(\frac{r^*\kappa}{\sqrt{A}}\right) - C_2 K_1\left(\frac{r^*\kappa}{\sqrt{A}}\right)\right] - \frac{Gr}{A}\left[\frac{C_7}{4}(2r^* \ln r^* - r^*) + C_8 \frac{r^*}{2}\right] \tag{32}$$

$$\tau_1 = \left.\frac{dU(R)}{dR}\right|_{R=1} = C_9 + \frac{E_z \Gamma \kappa}{\sqrt{A}}\left[C_1 I_1\left(\frac{\kappa}{\sqrt{A}}\right) - C_2 K_1\left(\frac{\kappa}{\sqrt{A}}\right)\right] + \frac{Gr}{A}\left[\frac{C_7}{4} - \frac{C_8}{2}\right] \tag{33}$$

Also, the volumetric flow rate in the microannulus is given in dimensionless form as:

$$Q = \int_0^1 RU(R)dR = C_9\left[\frac{(r^{*2} - 1)}{4} - \frac{r^{*2} \ln r^*}{2}\right] + C_{10}\frac{(1 - r^{*2})}{2}$$

$$-\frac{Gr}{A}\left[C_7\left(\left(\frac{r^{*4} - 1}{16}\right) - \frac{r^{*4} \ln r^*}{4}\right) + \frac{(1 - r^{*4})(C_8 - C_7)}{16}\right]$$

$$+\frac{E_z \Gamma \sqrt{A}}{\kappa}\left[C_1\left(I_1\left(\frac{\kappa}{\sqrt{A}}\right) - r^* I_1\left(\frac{r^*\kappa}{\sqrt{A}}\right)\right) - C_2\left(K_1\left(\frac{\kappa}{\sqrt{A}}\right) - r^* K_1\left(\frac{r^*\kappa}{\sqrt{A}}\right)\right)\right] \tag{34}$$

where

$$C_7 = \frac{r^*}{r^* \ln r^* - \alpha(1 - r^*)(r^* + 1)},$$

$$C_8 = C_7\left(\frac{1}{2} + \frac{r^{*2} \ln r^*}{1 - r^{*2}}\right),$$

$$C_9 = \frac{(Y_4 - Y_2) + (YY_4 - YY_2)Ez}{(Y_3 - Y_1)},$$

$$C_{10} = \frac{(Y_2Y_3 - Y_1Y_4) + (YY_2Y_3 - Y_1YY_4)Ez}{(Y_3 - Y_1)},$$

where $Y_{i's}$ are constants defined in the Appendix.

On applying the additional condition, $\int_{r^*}^{1} R\theta(R)dR = 0$, we obtain an expression for the degree of asymmetric heating as:

$$w = 1 + \frac{r^*}{r^* \ln r^* - \alpha(1-r^*)(r^*+1)}\left(\frac{1}{2} + \frac{r^{*2}\ln r^*}{1-r^{*2}} + \alpha(1-r^*)\right) \tag{35}$$

The novelty of this current investigation is the analytical computation of the induced streaming potential due to wall EDL. Following the work of Rice and Whitehead [10], the dimensional streaming current at the surfaces of the micro-annulus, induced by the EDL is defined as:

$$I_s = -\frac{2n_0zev}{H}\int_0^1 2\pi r u(r)\psi'(r)dr \tag{36}$$

Also, the streaming potential produces a conduction current in the reverse direction, which is given in dimensionless form as:

$$I_c = E_z'\lambda_0 A_c \tag{37}$$

where A_c is the cross-sectional area across the micro annulus and λ_0 is the electrical conductivity of the fluid. At steady-state, the sum of the streaming current and the electrical conduction current equals zero, so that

$$I_s + I_c = 0 \tag{38}$$

After further simplifications and applying equation (8), the dimensionless streaming potential is given as:

$$E_z = 2G_3\int_0^1 RU(R)\psi(R)dR \tag{39}$$

where $G_3 = \frac{zevL}{\lambda_0 A_c r_1}$ is a constant.

By obtaining the integral in equation (39), and solving for E_z, the dimensionless streaming potential (E_z) is obtained as:

$$E_z = \frac{Y_{13} + Y_{14}Y_7 + Y_{15}Y_9}{1 - (Y_{11} + Y_{12} + Y_{14}Y_8 + Y_{15}Y_{10})} \tag{40}$$

Equation (40) above represents the mathematical model for the induced streaming potential of natural convection flow in a vertical microannulus.

3. Results and discussion

To achieve the influence of electrokinetic phenomenon on natural convection flow in a microannulus, this section theoretical discuss and explicate the semi-analytical solutions obtained with the aid of line graphs by writing MATLAB codes for obtained solutions using MATLAB 2016a. The results obtained in this section deserve great attention as they tend to reduce the cost of undergoing an experiment to justify this impact. The solutions obtained illustrate that the basic governing parameters controlling flow formation and mass flow rate are dimensionless velocity-slip-length (α), dimensionless temperature-jump-length (δ), Debye-Hückel parameter (κ), annular gap (r^*), Grashof number (Gr), and magnitude of the electrokinetic force (Γ). It is desired to comprehend the role of these parameters on mass-flow rate enhancement and reduction of skin friction. Throughout this work, we have chosen the hydrodynamic slip length to be equal to thermal slip length ($\alpha = \delta$), $1 \leq \kappa \leq 100$, $-5 \leq Gr \leq 5$, $0.0 < r^* < 1$, $0 \leq \alpha \leq 0.1$.

Table 1 gives the numerical comparisons of transient volumetric flow rate with steady-state values. An excellent agreement is obtained for the steady-state values with those of transient state at large times. This agreement justifies the accuracy of RSA and the exact solution obtained at the steady-state.

Table 1. Numerical comparison of skin-friction and volumetric flow-rate for different values of t and κ

		RSA			Exact solution (SS)		
t	κ	$\tau_0(t, \kappa)$	$\tau_1(t, \kappa)$	$Q(t, \kappa)$	$\tau_0(\kappa)$	$\tau_1(\kappa)$	$Q(\kappa)$
	2.0	2.7502	2.2481	0.1701			
	5.0	12.3052	11.0050	0.7329			
	10.0	28.7137	27.4060	1.5625			
0.05	20.0	59.7472	60.0856	2.7624			
	30.0	91.2709	93.2952	3.8264			
	40.0	123.0312	126.7020	4.8562			
	50.0	154.8802	160.1831	5.8717			
	2.0	4.1100	3.1180	0.3241			
	5.0	18.5516	15.7607	1.1939			
	10.0	41.9734	37.7555	2.4645			
0.5	20.0	82.7470	78.2311	4.2771			
	30.0	122.8176	118.2852	5.8780			
	40.0	162.8743	158.3355	7.4285			
	50.0	202.9308	198.3884	8.9590			
	2.0	4.0233	3.0486	0.2341	4.0234	3.0487	0.2340
	5.0	18.4624	15.6886	1.1037	18.4623	15.6886	1.1037
	10.0	41.8762	37.6754	2.3742	41.8762	37.6753	2.3741
SS	20.0	82.6236	78.1240	4.1864	82.6234	78.1241	4.1864
	30.0	122.6574	118.1408	5.7872	122.6574	118.1408	5.7871
	40.0	162.6702	158.1462	7.3374	162.6703	158.1463	7.3374
	50.0	202.6781	198.1495	8.8675	202.6782	198.1496	8.8676

Figure 2 depicts electric potential in the microchannel for different values of κ. It is evident from this figure that the electric potential due to EDL decreases with an increase in κ. This is physically true since an increase in κ corresponds to a smaller EDL at the microannulus surfaces. It is important to state that as $\kappa \to \infty$, the electrokinetic phenomenon vanishes in the microannulus. This is because κ is inversely proportional to EDL length.

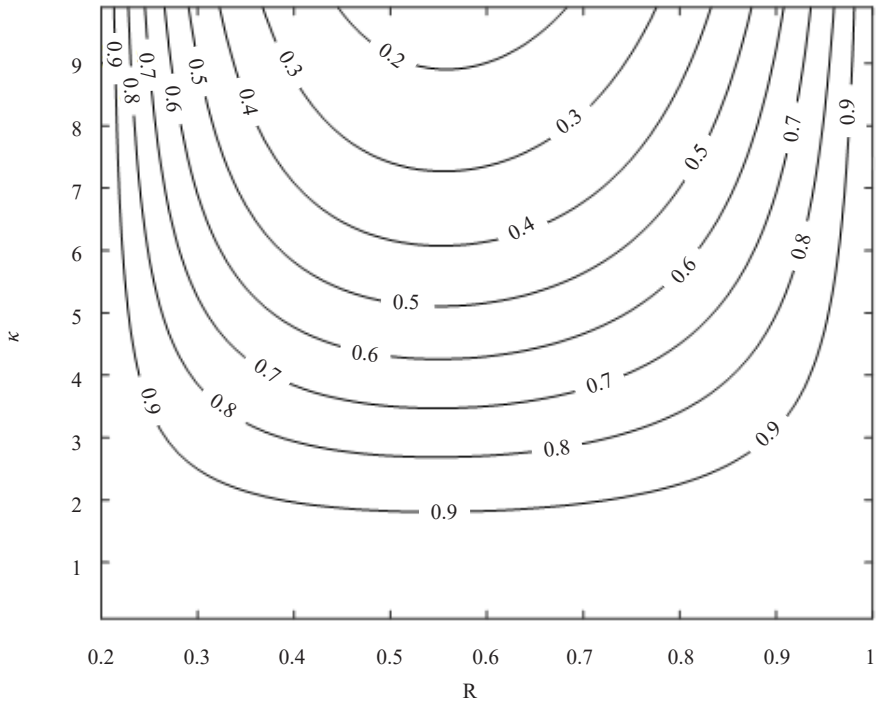

Figure 2. Electric potential for different values κ

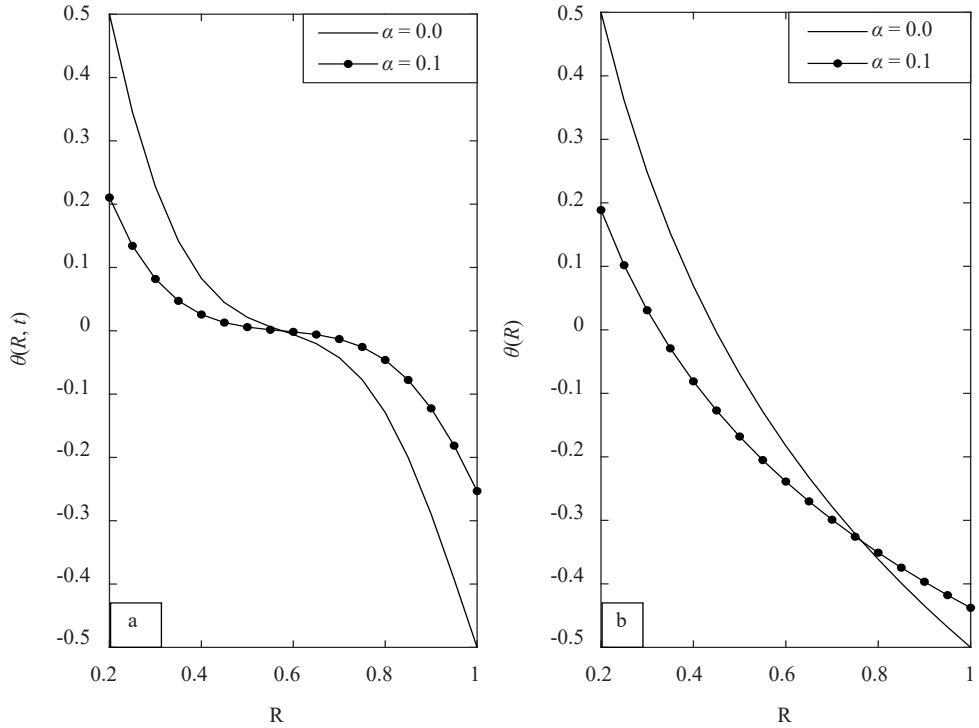

Figure 3. Temperature distribution for (a) transient state, (b) steady-state for different values of α

To establish the objective of this current article, Figures 3-5 present a comparative study of transient and steady-state representation for temperature distribution, velocity profile, skin friction, and volumetric flow rate. In all the

figures, it is obvious that the transient state solutions (time-dependent) are significantly different from those of steady-state. A careful look at the figures indicates that the temperature, velocity, and skin friction at the surfaces of the micro-annulus and volumetric flow rate attain steady-state solutions at large times. Figure 4 demonstrated that the maximum velocity is obtained when the slip-velocity at the microannulus surfaces is incorporated into the mathematical model at the steady-state.

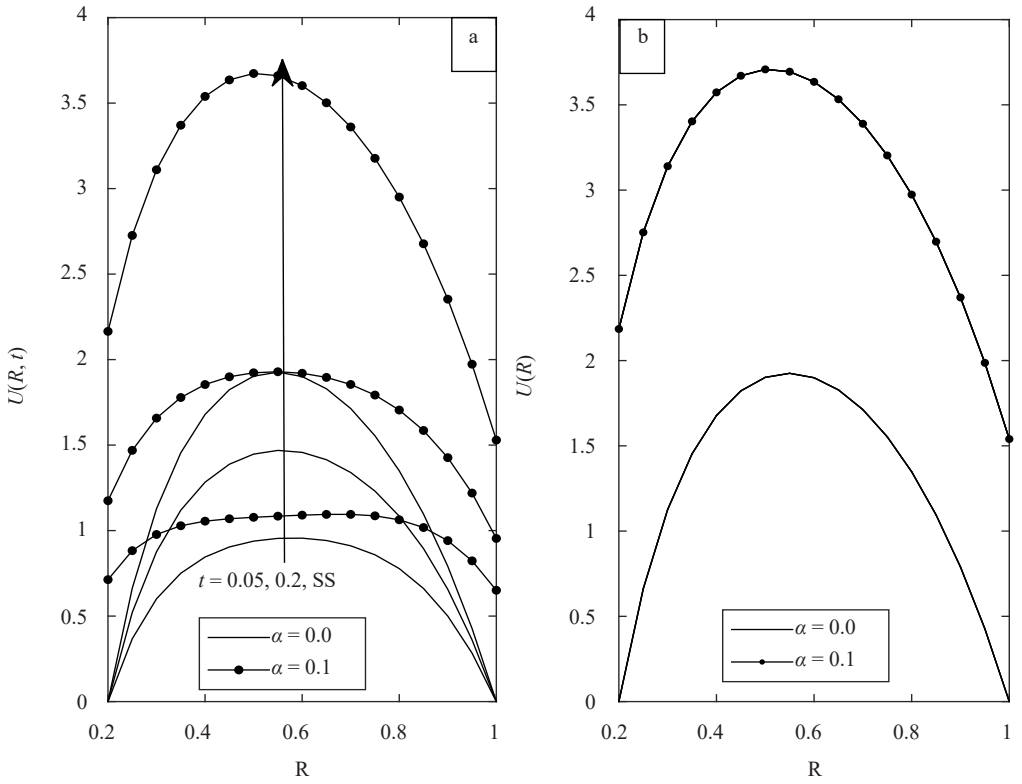

Figure 4. Temperature distribution for (a) transient state, (b) steady-state for different values of α

On the other hand, Figure 5 displays the skin friction at the outer surface of the inner cylinder at different times. It is also observable that the skin friction for slip-flow is considerably lower than the no-slip condition. This could have led to the overestimation of skin friction by the design engineer, should the velocity slip at the surfaces of the micro-annulus has been neglected.

A very significant analysis in this current work is the computation of the volumetric flow rate. Figures 6 and 10 demonstrate the role of time, velocity slip (α), Grashof number (Gr), and annular gap (r^*) at transient and steady-state respectively. Figure 6 clarifies that the role of time and velocity slip is to enhance volumetric flow rate throughout the microchannel. This could be attributed to the fact that an increase in α increases the velocity slip-length and therefore increases the free mean path of the fluid molecule. A point of intersection is found around $\kappa = 15$, between the steady-state solution of the no-slip condition and the transient state of the slip flow. At this point, the volumetric flow rate is independent of flow regimes. Figure 10 on the other hand depicts the steady-state volumetric flow rate for different values of α, Gr, and r^*. The volumetric flow rate is found to be an increasing function of r^* regardless of the flow regime. This finding suggests that for buoyancy opposed flow, the EDL length and electric potential act as enhancers of volumetric flow rate when the application of pressure is unachievable.

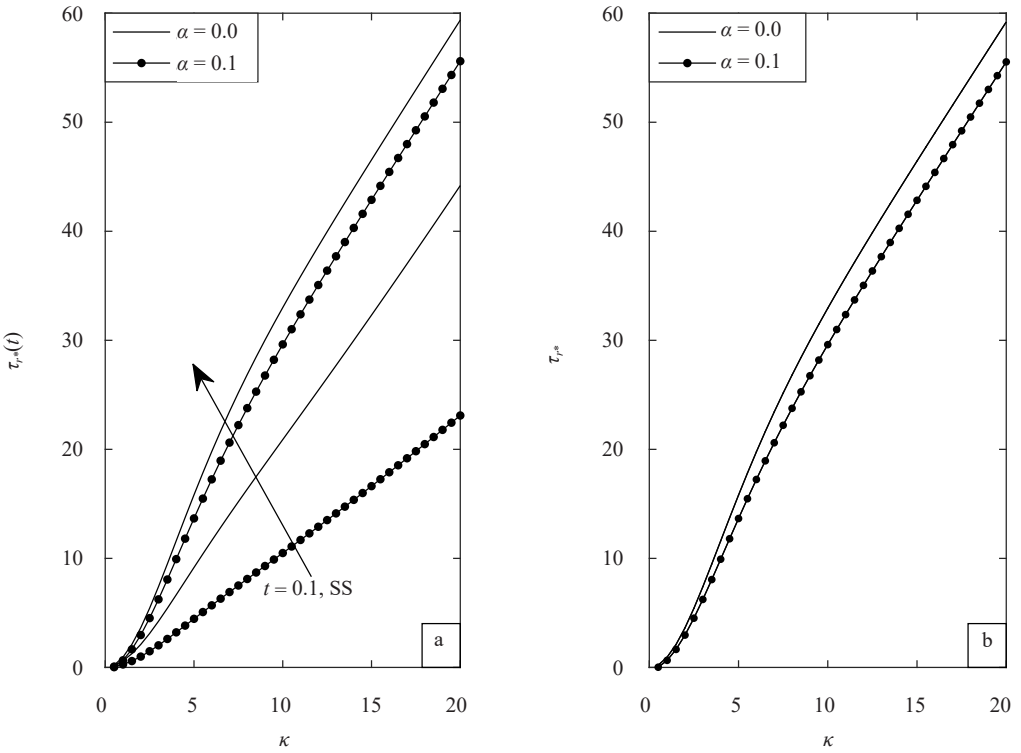

Figure 5. Skin-friction for (a) transient state, (b) steady-state for different values of α

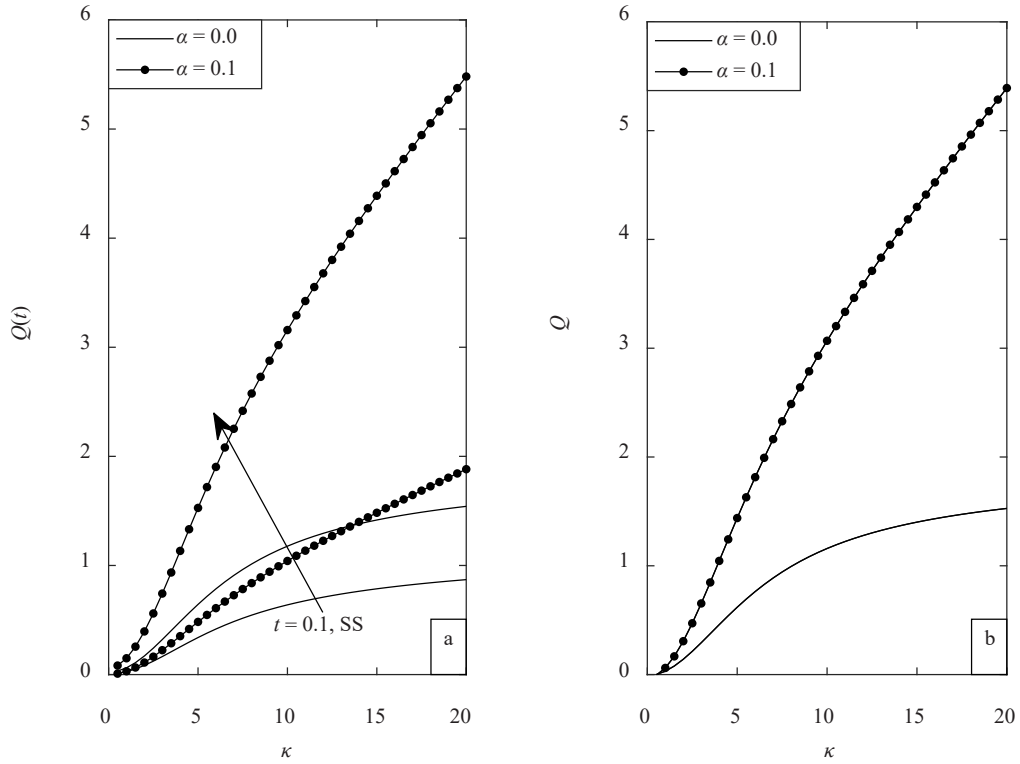

Figure 6. Volumetric flow rate for (a) transient state, (b) steady-state for different values of α

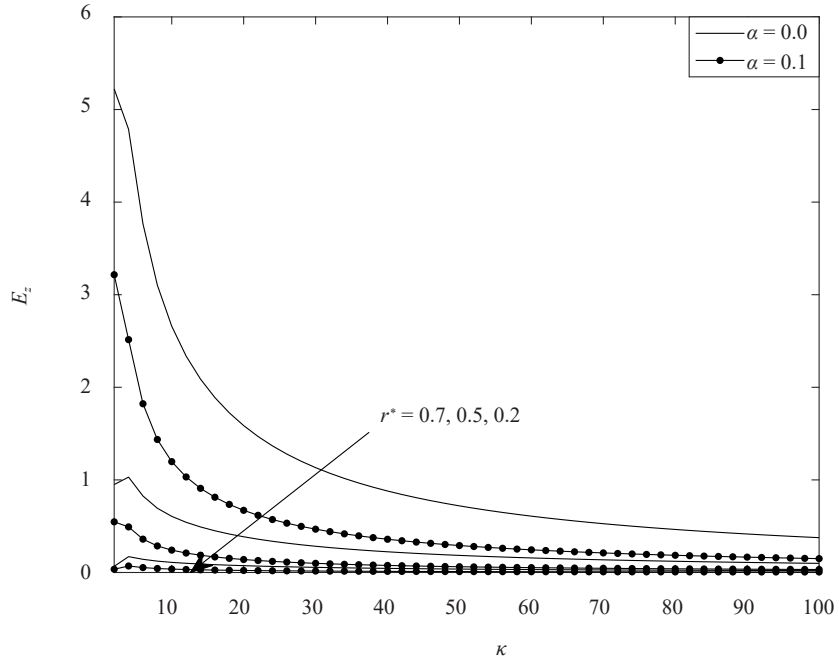

Figure 7. Electric field strength for different values of α and r^*

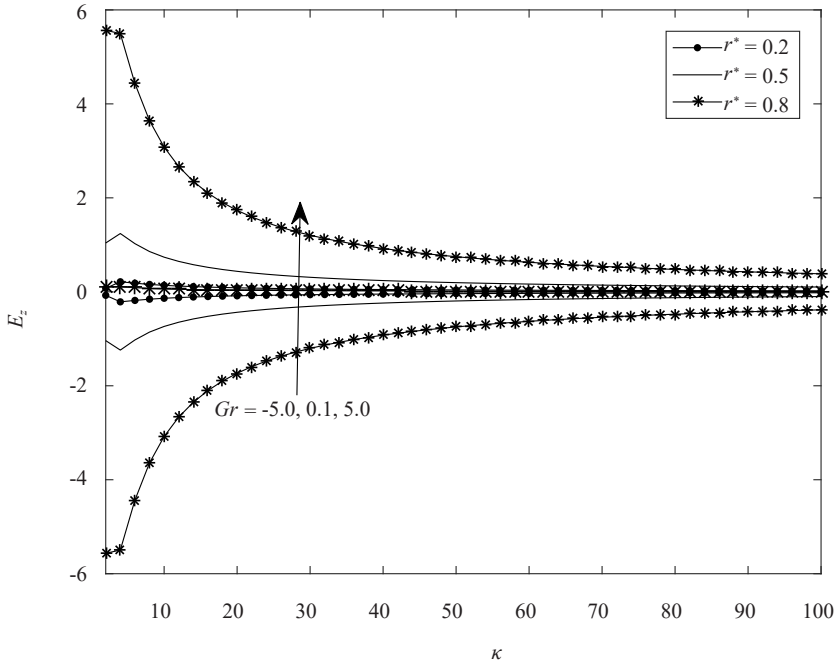

Figure 8. Electric field strength for different values of Gr and r^*

Another noteworthy interest in this article is understanding the streaming potential, which is induced when streaming current and electrical conduction current are equal. Figure 7 illustrates the impact of α, Gr, and r^* on the induced streaming potential. It is found from this figure that the maximum streaming potential is found for large EDL (corresponding to a small value of κ) and decreases with an increase in κ. In addition, since an increase in the annular gap corresponds to a decrease in r^*, the streaming potential can be enhanced by considering a tinier annular gap. This

could be attributed to the fact that an increase in r^* leads to a decrease in the microannulus width thereby amplifying the EDL size which in turn enhances the induced streaming potential. Figure 8 on the other hand explicates the impact of on the dimensionless streaming potential. It is found from this figure that the streaming potential decreases for buoyancy assisted flow ($Gr > 0$) and otherwise for ($Gr < 0$) as κ increases. It is important to state here that negative Gr implies that buoyant force acts in opposite direction to flow direction.

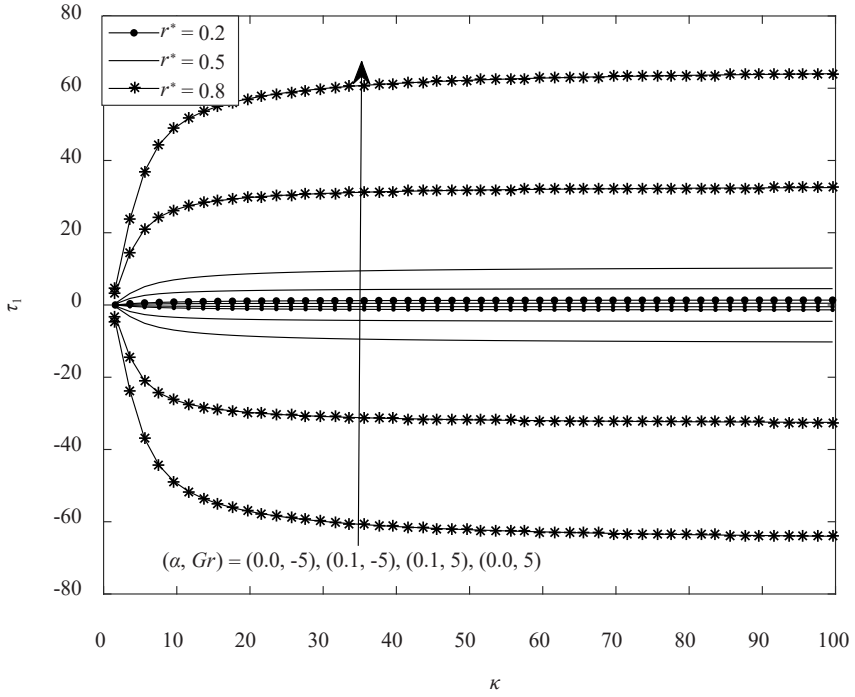

Figure 9. Skin-friction at the inner surface of outer cylinder for different values of α, Gr, and r^*

Figure 9 presents the skin-fiction at the inner surface of the outer cylinder as a function of α, Gr, and r^* It is found from this figure that the skin friction is higher for buoyancy assisted flow ($Gr > 0$) and otherwise for ($Gr < 0$) as κ increases. Also, for $Gr = 0$ the skin friction is found to reduce to zero. In addition, skin friction at this surface can be suppressed by increasing the annular gap ($r^* \rightarrow 0$).

4. Conclusion

This article theoretically established the impact of the electrokinetic phenomenon on time-dependent natural convection flow in a microannulus with velocity slip and temperature jump. The following major conclusions are drawn based on simulated results:

I. Fluid velocity, temperature distribution, and mass flow rate at transient state are significantly different from steady-state values.

II. The volumetric flow rate would have been underestimated, should the slip conditions at the microannulus surfaces had not been considered.

III. The role of microannulus EDL is to increase skin friction as well as volumetric flow rate.

IV. Increase in annular gap decreases induced streaming potential, skin friction, and volumetric flow rate in the microannulus.

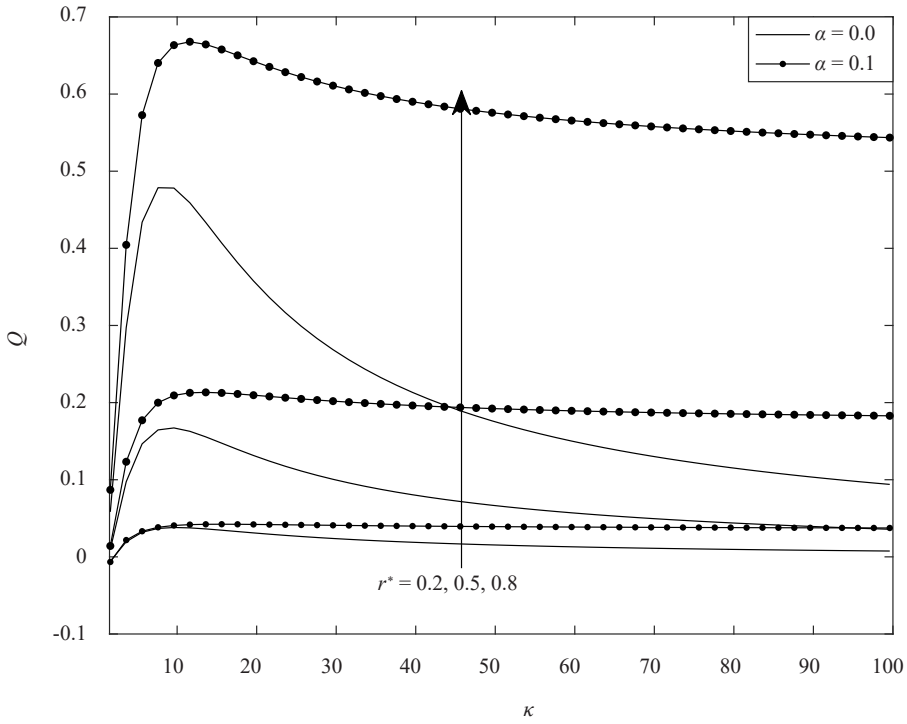

Figure 10. Volumetric flow rate for different values of r^*

Conflict of interest

The authors declare that they have no conflict of interest.

References

[1] S. C. Terry, J. H. Jerman, and J. B. Angell, "A gas chromatographic air analyzer fabricated on a silicon wafer," *IEEE Transactions on Electron Devices*, vol. 26, no. 12, pp. 1880-1886, 1979.

[2] B. J. Kirby, *Micro- and Nanoscale Fluid Mechanics: Transport in Microfluidic Devices*. Chicago: Cambridge University Press, 2010.

[3] G. M. Karniadakis, A. Beskok, and N. Aluru, *Microflows and Nanoflows*. Springer Verlag, 2005.

[4] F. F. Reuss, "Sur un nouvel effet de l'électricité galvanique (in French)," *Mémoires de la Société Impériale des Naturalistes de Moscou* (in French), vol. 2, pp. 327-337, 1809.

[5] R. F. Probstein, *Physicochemical Hydrodynamics: An Introduction*. New York: John Wiley& Sons, Inc., 1994.

[6] G. M. Mala, D. Li, C. Werner, H. J. Jacobasch, and Y. B. Ning, "Flow characteristics of water through a microchannel between two parallel plates with electrokinetic effects," *International Journal of Heat and Fluid Flow*, vol. 18, no. 5, pp. 489-496, 1997.

[7] G. M. Mala, D. Li, and J. D. Dale, "Heat transfer and fluid flow in microchannels," *International Journal of Heat and Mass Transfer*, vol. 40, no. 13, pp. 3079-3088, 1997.

[8] L. Ren, W. Qu, and D. Li, "Interfacial electrokinetic effects on liquid flow in microchannels," *International Journal of Heat and Mass Transfer*, vol. 44, no. 16, pp. 3125-3134, 2001.

[9] Y. P. Zhang, T. W. Xu, and Z. H. Liu, "Streaming potential across a porous charged membrane in organic-aqueous solutions," *Desalination*, vol. 212, no. 1-3, pp. 183-190, 2007.

[10] C. L. Rice and R. Whitehead, "Electrokinetic flow in a narrow cylindrical capillary," *The Journal of Physical Chemistry*, vol. 69, no. 11, pp. 4017-4024, 1965.

[11] D. Burgreen and F. R. Nakache, "Electrokinetic flow in ultrafine capillary slits," *The Journal of Physical Chemistry*, vol. 68, pp. 1084-1091, 1964.

[12] S. Levine, J. R. Marriott, G. Neale, and N. Epstein, "Theory of electrokinetic flow in fine cylindrical capillaries at high zeta-potentials," *Journal of Colloid Interface Science*, vol. 52, pp. 136-149, 1974.
[13] B. C. Liechty, B. W. Webb, and R. D. Maynes, "Convective heat transfer characteristics of electro-osmotically generated flow in microtubes at high wall potential," *International Journal of Heat and Mass Transfer*, vol. 48, pp. 2360-2371, 2005.
[14] P. Debye and H. Hückel, "The theory of electrolytes. I. Lowering of freezing point and related phenomena," *Physikalische Zeitschrift*, vol. 24, pp. 185-206, 1923.
[15] X. P. Wang, H. T. Qi, and H. Y. Xu, "Transient electroosmotic flow of generalized second grade fluids under slip boundary conditions," *Canadian Journal of Physics*, vol. 99, pp. 1-10, 2017.
[16] X. Yang, H. T. Qi, and X. Y. Jiang, "Numerical analysis for electroosmotic flow of fractional Maxwell fluids," *Applied Mathematics Letters*, vol. 78, pp. 1-8, 2018.
[17] B. K. Jha and M. O. Oni, "Theoretical analysis of transient natural convection flow in a vertical microchannel with electrokinetic effect," *Journal of Taibah University for Science*, vol. 13, no. 1, pp. 1087-1099, 2019.
[18] R. J. Yang, L. M. Fu, and Y. C. Lin, "Electroosmotic flow in microchannels," *Journal of Colloid Interface Science*, vol. 239, pp. 98-105, 2001.
[19] C. Y. Soong and S. H. Wang, "Theoretical analysis of electrokinetic flow and heat transfer in a microchannel under asymmetric boundary conditions," *Journal of Colloid Interface Science*, vol. 256, pp. 202-213, 2003.
[20] A. Mukhopadhyay, S. Banerjee, and C. Gupta, "Fully developed hydrodynamic and thermal transport in combined pressure and electrokinetically driven flow in a microchannel with a symmetric boundary conditions," *International Journal of Heat and Mass Transfer*, vol. 52, pp. 2145-2154, 2009.
[21] C. Yang and D. Q. Li, "Analysis of electrokinetic effects on the liquid flow in rectangular microchannels," *Colloids and Surfaces A: Physicochemical and Engineering Aspects*, vol. 143, no. 2, pp. 339-353, 1998.
[22] B. K. Jha and M. O. Oni, "Natural convection flow in a vertical tube inspired by time-periodic heating," *Alexandria Engineering Journal*, vol. 55, no. 4, pp. 3145-3151, 2016.
[23] B. K. Jha and M. O. Oni, "Transient natural convection flow between vertical concentric cylinders heated/cooled asymmetrically," *Proceedings of the Institution of Mechanical Engineers, Part A: Journal of Power and Energy*, vol. 232, no. 7, pp. 926-939, 2018.
[24] T. T. Kao, "Laminar free convective heat transfer response along a vertical flat plate with step jump in surface temperature," *Letters in Heat and Mass Transfer*, vol. 2, no. 5, pp. 419-428, 1975.
[25] B. K. Jha and M. O. Oni, "Electromagnetic natural convection flow in a vertical microchannel with Joule heating: An exact solution," *Journal of Taibah University for Science*, vol. 12, no. 5, pp. 661-668, 2018.
[26] B. K. Jha, M. O. Oni, and B. Aina, "Steady fully developed mixed convection flow in a vertical micro-concentric-annulus with heat generating/absorbing fluid: an exact solution," *Ain Shams Engineering Journal*, 2016.
[27] B. K. Jha and M. O. Oni, "Natural convection flow in a vertical annulus with time-periodic thermal boundary conditions," *Propulsion and Power Research*, vol. 8, no. 1, pp. 47-55, 2019.
[28] C. K. Chen and H. C. Weng, "Natural convection flow in a vertical microchannel," *Journal of Heat Transfer*, vol. 127, pp. 1053-1059, 2005.
[29] A. Barletta and E. Zanchini, "On the choice of the reference temperature for fully developed mixed convection flow in a vertical channel," *International Journal of Heat and Mass Transfer*, vol. 42, pp. 3169-3181, 1999.
[30] M. Avci and O. Aydin, "Mixed convection in a vertical parallel plate microchannel with asymmetric wall heat fluxes," *ASME Journal of Heat Transfer*, vol. 129, no. 8, pp. 1091-1095, 2007.
[31] N. M. D. Khan, H. Xu, Q. Zhao, and Q. Sun, "Analysis of mixed convection in a vertical channel in the presence of electrical double layers," *Zeitschrift für Naturforschung A*, vol. 73, no. 8, pp. 741-751, 2018.
[32] M. O. Oni and B. K. Jha, "Theoretical analysis of transient natural convection flow in a vertical microchannel with electrokinetic effect," *Journal of Taibah University for Science*, vol. 13 no. 1, pp. 1087-1099, 2019.
[33] T. S. Davi, C. V. Lakshmi, K. Venkatadri, and M. S. Reddy, "Influence of external magnetic wire on natural convection of non-Newtonian fluid in a square cavity," *Partial Differential Equations in Applied Mathematics*, vol. 4. pp. 100041, 2021.
[34] B. S. Goud, P. P. Kumar, and B. S. Malga, "Effect of heat source on an unsteady MHD free convection flow of Casson fluid past a vertical oscillating plate in porous medium using finite element analysis," *Partial Differential Equations in Applied Mathematics*, vol. 2, pp. 100015, 2020.
[35] L. Gai, M. Li, and B. Sudao, "Approximate analytical and numerical solutions of a nonlinear boundary value problem in fluid mechanics based on symmetry reduction," *Partial Differential Equations in Applied Mathematics*, vol. 2, pp. 100011, 2020.

[36] A. Rahmat, N. Tofighi, M. S. Shadloo, and Z. Yildiz, "Numerical simulation of wall bounded and electrically excited Rayleigh-Taylor instability using incompressible smoothed particle hydrodynamics," *Colloids and Surfaces A: Physicochemical and Engineering Aspects*, vol. 460, pp. 60-70, 2014.
[37] T. Abdulrazzaq, H. Togun, M. Goodarzi, S. N. Kazi, M. K. Ariffin, N. M. Adam, and K. Hooman, "Turbulent heat transfer and nanofluid flow in an annular cylinder with sudden reduction," *Journal of Thermal Analysis and Calorimetry*, vol. 141, no. 1, pp. 373-385, 2020.
[38] Y. A. Elmaboud, "Two-layered electroosmotic flow through a vertical microchannel with fractional Cattaneo heat flux," *Journal of Taibah University for Science*, vol. 15, no. 1, pp. 1038-1053, 2021.
[39] A. I. Abdellateef, H. M. Alshehri, and Y. A. Elmaboud, "Electro-osmotic flow of fractional second-grade fluid with fractional Cattaneo heat flux through a vertical microchannel," *Heat Transfer*, vol. 50, no. 7, pp. 6628-6644, 2021.
[40] A. M. Alsharif and Y. A. Elmaboud, "Electroosmotic flow of generalized fractional second grade fluid with fractional Cattaneo model through a vertical annulus," *Chinese Journal of Physics*, 2021. [Online serial]. Available: https://doi.org/10.1016/j.cjph.2021.08.021. [Accessed Oct. 30, 2021].
[41] M. O. Oni and B. K. Jha, "Electroosmotic natural convection flow in a vertical microchannel with asymmetric heat fluxes," *SN Applied Sciences*, vol. 2, no. 10, pp. 1-14, 2020.
[42] M. O. Oni and B. K. Jha, "Joule heating and viscous dissipation effect on electroosmotic mixed convection flow in a vertical microchannel subjected to asymmetric heat fluxes," *Propulsion and Power Research*, vol. 10, no. 1, pp. 83-94, 2021.
[43] M. Avci and O. Aydin, "Mixed convection in a vertical microannulus between two concentric microtubes," *ASME Journal of Heat Transfer*, vol. 131, pp. 014502-014504, 2009.
[44] B. K. Jha and C. A. Apere, "Unsteady MHD couette flow in annuli: the riemann-sum approximation approach," *Journal of Physical Society of Japan*, vol. 79, no. 12, pp. 124403, 2010.
[45] B. K. Jha and M. O. Oni, "An analytical solution for temperature field around a cylindrical surface subjected to a time dependent heat flux: An alternative approach," *Alexandria Engineering Journal*, vol. 57, no. 2, pp. 927-929, 2017.
[46] A. F. Khadrawi and M. A. Al-Nimr, "Unsteady natural convection fluid flow in a vertical microchannel under the effect of the Dual-phase-Lag heat conduction model," *International Journal of Thermophysics*, vol. 28, no. 4, pp. 1387-1400, 2007.
[47] D. Y. Tzou, *Macro to Microscale Heat Transfer: The Lagging Behaviour*. Washington: Taylor and Francis, 1997.

Appendix

$$X_1 = I_0\left(r^*\sqrt{\frac{sPr}{A}}\right) - \delta(1-r^*)\sqrt{\frac{sPr}{A}}I_1\left(r^*\sqrt{\frac{sPr}{A}}\right),$$

$$X_2 = K_0\left(r^*\sqrt{\frac{sPr}{A}}\right) + \delta(1-r^*)\sqrt{\frac{sPr}{A}}K_1\left(r^*\sqrt{\frac{sPr}{A}}\right),$$

$$X_3 = \frac{w}{s},$$

$$X_4 = I_0\left(\sqrt{\frac{sPr}{A}}\right) + \delta(1-r^*)\sqrt{\frac{sPr}{A}}I_1\left(\sqrt{\frac{sPr}{A}}\right),$$

$$X_5 = K_0\left(\sqrt{\frac{sPr}{A}}\right) - \delta(1-r^*)\sqrt{\frac{sPr}{A}}K_1\left(\sqrt{\frac{sPr}{A}}\right),$$

$$X_6 = \frac{w-1}{s},$$

$$X_{10} = I_0\left(r^*\sqrt{\frac{s}{A}}\right) - \alpha(1-r^*)\sqrt{\frac{s}{A}}I_1\left(r^*\sqrt{\frac{s}{A}}\right),$$

$$X_{11} = K_0\left(r^*\sqrt{\frac{s}{A}}\right) + \alpha(1-r^*)\sqrt{\frac{s}{A}}K_1\left(r^*\sqrt{\frac{s}{A}}\right),$$

$$X_{12} = \frac{Gr}{s(Pr-1)}\left[C_3 I_0\left(r^*\sqrt{\frac{sPr}{A}}\right) + C_4 K_0\left(r^*\sqrt{\frac{sPr}{A}}\right)\right]$$

$$-\frac{aGr(1-r^*)}{s(Pr-1)}\sqrt{\frac{sPr}{A}}\left[C_3 I_1\left(r^*\sqrt{\frac{sPr}{A}}\right) - C_4 K_1\left(r^*\sqrt{\frac{sPr}{A}}\right)\right],$$

$$X_{13} = -\frac{\Gamma\kappa^2}{s(k^2-s)}\left[C_1 I_0\left(\frac{r^*\kappa}{\sqrt{A}}\right) + C_2 K_0\left(\frac{r^*\kappa}{\sqrt{A}}\right)\right] + \frac{a\Gamma\kappa^3(1-r^*)}{s(k^2-s)\sqrt{A}}\left[C_1 I_1\left(\frac{r^*\kappa}{\sqrt{A}}\right) - C_2 K_1\left(\frac{r^*\kappa}{\sqrt{A}}\right)\right],$$

$$X_{14} = I_0\left(\sqrt{\frac{s}{A}}\right) + \alpha(1-r^*)\sqrt{\frac{s}{A}}I_1\left(\sqrt{\frac{s}{A}}\right),$$

$$X_{15} = K_0\left(\sqrt{\frac{s}{A}}\right) - \alpha(1-r^*)\sqrt{\frac{s}{A}}K_1\left(\sqrt{\frac{s}{A}}\right),$$

$$X_{16} = \frac{Gr}{s(Pr-1)}\left[C_3 I_0\left(\sqrt{\frac{sPr}{A}}\right) + C_4 K_0\left(\sqrt{\frac{sPr}{A}}\right)\right] + \frac{aGr(1-r^*)}{s(Pr-1)}\sqrt{\frac{sPr}{A}}\left[C_3 I_1\left(\sqrt{\frac{sPr}{A}}\right) - C_4 K_1\left(\sqrt{\frac{sPr}{A}}\right)\right],$$

$$X_{17} = -\frac{\Gamma\kappa^2}{s(k^2-s)}\left[C_1 I_0\left(\frac{\kappa}{\sqrt{A}}\right) + C_2 K_0\left(\frac{\kappa}{\sqrt{A}}\right)\right] - \frac{a\Gamma\kappa^3(1-r^*)}{s(k^2-s)\sqrt{A}}\left[C_1 I_1\left(\frac{\kappa}{\sqrt{A}}\right) - C_2 K_1\left(\frac{\kappa}{\sqrt{A}}\right)\right],$$

$$Y_1 = \ln r^* - \frac{\alpha(1-r^*)}{r^*},$$

$$Y_2 = \frac{Gr}{4A}\left[Y_5 - \alpha(1-r^*)Y_6\right],$$

$$Y_3 = \alpha(1-r^*),$$

$$Y_4 = \frac{Gr}{4A}\left[C_8 - C_7 + \alpha(1-r^*)(2C_8 - C_7)\right],$$

$$Y_5 = C_7 r^{*2}(\ln r^* - 1) + C_8 r^{*2},$$

$$YY_2 = \Gamma\left[\frac{\alpha\kappa(1-r^*)}{\sqrt{A}}\left(C_1 I_1\left(\frac{r^*\kappa}{\sqrt{A}}\right) - C_2 K_1\left(\frac{r^*\kappa}{\sqrt{A}}\right)\right) - C_1 I_0\left(\frac{r^*\kappa}{\sqrt{A}}\right) + C_2 K_0\left(\frac{r^*\kappa}{\sqrt{A}}\right)\right],$$

$$YY_4 = \Gamma\left[\frac{\alpha\kappa(r^*-1)}{\sqrt{A}}\left(C_1 I_1\left(\frac{\kappa}{\sqrt{A}}\right) - C_2 K_1\left(\frac{\kappa}{\sqrt{A}}\right)\right) - C_1 I_0\left(\frac{\kappa}{\sqrt{A}}\right) + C_2 K_0\left(\frac{\kappa}{\sqrt{A}}\right)\right],$$

$$Y_6 = C_7 r^*(2\ln r^* - 1) + 2C_8 r^*,$$

$$Y_7 = \frac{Y_4 - Y_2}{Y_3 - Y_1},$$

$$Y_8 = \frac{YY_4 - YY_2}{Y_3 - Y_1},$$

$$Y_9 = \frac{Y_2 Y_3 - Y_1 Y_4}{Y_3 - Y_1},$$

$$Y_{10} = \frac{YY_2Y_3 - Y_1YY_4}{Y_3 - Y_1},$$

$$Y_{11} = 2G_3\Gamma C_1^2 \left\{ \frac{\left[I_0^2\left(\frac{\kappa}{\sqrt{A}}\right) - I_1^2\left(\frac{\kappa}{\sqrt{A}}\right)\right]}{2} - r^{*2}\frac{\left[I_0^2\left(\frac{r^*\kappa}{\sqrt{A}}\right) - I_1^2\left(\frac{r^*\kappa}{\sqrt{A}}\right)\right]}{2} \right\}$$

$$+2G_3\Gamma C_2^2 \left\{ \frac{\left[K_0^2\left(\frac{\kappa}{\sqrt{A}}\right) - K_1^2\left(\frac{\kappa}{\sqrt{A}}\right)\right]}{2} - r^{*2}\frac{\left[K_0^2\left(\frac{r^*\kappa}{\sqrt{A}}\right) - K_1^2\left(\frac{r^*\kappa}{\sqrt{A}}\right)\right]}{2} \right\},$$

$$Y_{12} = 4G_3\Gamma C_1C_2 \left\{ \frac{\left[I_0\left(\frac{\kappa}{\sqrt{A}}\right)K_0\left(\frac{\kappa}{\sqrt{A}}\right) + I_1\left(\frac{\kappa}{\sqrt{A}}\right)K_1\left(\frac{\kappa}{\sqrt{A}}\right)\right]}{2} - \frac{r^{*2}\left[I_0\left(\frac{r^*\kappa}{\sqrt{A}}\right)K_0\left(\frac{r^*\kappa}{\sqrt{A}}\right) + I_1\left(\frac{r^*\kappa}{\sqrt{A}}\right)K_1\left(\frac{r^*\kappa}{\sqrt{A}}\right)\right]}{2} \right\},$$

$$Y_{13} = 4G_3 \left\{ \frac{GrC_1C_7}{4A} \left[\frac{4I_0\left(\frac{\kappa}{\sqrt{A}}\right)}{\kappa^4} + \frac{I_0\left(\frac{\kappa}{\sqrt{A}}\right)}{\kappa^2} - \frac{4I_1\left(\frac{\kappa}{\sqrt{A}}\right)}{\kappa^3} \right.\right.$$

$$+\ln r^* \left[\frac{4r^*I_1\left(\frac{r^*\kappa}{\sqrt{A}}\right)}{\kappa^3} - \frac{2r^{*2}I_0\left(\frac{r^*\kappa}{\sqrt{A}}\right)}{\kappa^2} + \frac{r^{*3}I_1\left(\frac{r^*\kappa}{\sqrt{A}}\right)}{\kappa} \right]$$

$$\left.\left. - \frac{4I_0\left(\frac{r^*\kappa}{\sqrt{A}}\right)}{\kappa^4} - \frac{r^{*2}I_0\left(\frac{r^*\kappa}{\sqrt{A}}\right)}{\kappa^2} + \frac{4r^*I_1\left(\frac{r^*\kappa}{\sqrt{A}}\right)}{\kappa^3} \right] \right.$$

$$+\frac{GrC_1(C_7 - C_8)}{4A} \left[\frac{1}{\kappa}\left(\frac{4}{\kappa^2} + 1\right)I_1\left(\frac{\kappa}{\sqrt{A}}\right) - \frac{2I_0\left(\frac{\kappa}{\sqrt{A}}\right)}{\kappa} - \frac{r^*}{\kappa}\left(\frac{4}{\kappa^2} + r^{*2}\right)I_1\left(\frac{r^*\kappa}{\sqrt{A}}\right) - \frac{2r^*I_0\left(\frac{\kappa}{\sqrt{A}}\right)}{\kappa} \right]$$

$$+\frac{GrC_2C_7}{4A} \left[\frac{4K_1\left(\frac{\kappa}{\sqrt{A}}\right)}{\kappa^3} + \frac{K_0\left(\frac{\kappa}{\sqrt{A}}\right)}{\kappa^2} - \frac{4K_0\left(\frac{\kappa}{\sqrt{A}}\right)}{\kappa^4} \right.$$

$$-\ln r^*\left[\frac{4r^*K_1\left(\frac{r^*\kappa}{\sqrt{A}}\right)}{\kappa^3}+\frac{2r^{*2}K_0\left(\frac{r^*\kappa}{\sqrt{A}}\right)}{\kappa^2}+\frac{r^{*3}K_1\left(\frac{r^*\kappa}{\sqrt{A}}\right)}{\kappa}\right]$$

$$+\frac{4K_0\left(\frac{r^*\kappa}{\sqrt{A}}\right)}{\kappa^4}+\frac{r^{*2}K_0\left(\frac{r^*\kappa}{\sqrt{A}}\right)}{\kappa^2}+\frac{4r^*K_1\left(\frac{r^*\kappa}{\sqrt{A}}\right)}{\kappa^3}\Bigg]$$

$$+\frac{GrC_2(C_7-C_8)}{4A}\left[-\frac{1}{\kappa}\left(\frac{4}{\kappa^2}+1\right)K_1\left(\frac{\kappa}{\sqrt{A}}\right)+\frac{2K_0\left(\frac{\kappa}{\sqrt{A}}\right)}{\kappa}+\frac{r^*}{\kappa}\left(\frac{4}{\kappa^2}+r^{*2}\right)K_1\left(\frac{r^*\kappa}{\sqrt{A}}\right)+\frac{2r^*K_0\left(\frac{\kappa}{\sqrt{A}}\right)}{\kappa}\right]\Bigg\},$$

$$Y_{14}=2G_3\left\{C_1\left[\frac{I_0\left(\frac{r^*\kappa}{\sqrt{A}}\right)}{\kappa^2}-\frac{r^*\ln r^*I_1\left(\frac{r^*\kappa}{\sqrt{A}}\right)}{\kappa}-\frac{I_0\left(\frac{\kappa}{\sqrt{A}}\right)}{\kappa^2}\right]\right.$$

$$\left.+C_2\left[\frac{K_0\left(\frac{r^*\kappa}{\sqrt{A}}\right)}{\kappa^2}+\frac{r^*\ln r^*K_1\left(\frac{r^*\kappa}{\sqrt{A}}\right)}{\kappa}-\frac{K_0\left(\frac{\kappa}{\sqrt{A}}\right)}{\kappa^2}\right]\right\},$$

$$Y_{15}=2G_3\left\{C_1\left[\frac{I_1\left(\frac{r^*\kappa}{\sqrt{A}}\right)}{\kappa}-\frac{r^*I_1\left(\frac{r^*\kappa}{\sqrt{A}}\right)}{\kappa}\right]+C_2\left[\frac{K_1\left(\frac{r^*\kappa}{\sqrt{A}}\right)}{\kappa}-\frac{r^*K_1\left(\frac{r^*\kappa}{\sqrt{A}}\right)}{\kappa}\right]\right\},$$

$$Y_{16}=Y_{13}+Y_{14}Y_7+Y_{15}Y_9,$$

$$Y_{17}=1-(Y_{11}+Y_{12}+Y_{14}Y_8+Y_{15}Y_{10})$$